Crystal engineering of two light and pressure responsive physisorbents

Porous Materials Hot Paper

How to cite:
International Edition: doi.org/10.1002/anie.202219039
German Edition: doi.org/10.1002/ange.202219039

Crystal Engineering of Two Light and Pressure Responsive Physisorbents

*Dominic C. Castell[+], Varvara I. Nikolayenko[+], Debobroto Sensharma, Kyriaki Koupepidou, Katherine A. Forrest, Carlos J. Solanilla-Salinas, Brian Space, Leonard J. Barbour, and Michael J. Zaworotko**

Abstract: An emerging strategy in the design of efficient gas storage technologies is the development of stimuli-responsive physisorbents which undergo transformations in response to a particular stimulus, such as pressure, heat or light. Herein, we report two isostructural light modulated adsorbents (LMAs) containing bis-3-thienylcyclopentene (BTCP), **LMA-1 [Cd(BTCP)(DPT)$_2$]** (DPT = 2,5-diphenylbenzene-1,4-dicarboxylate) and **LMA-2 [Cd(BTCP)(FDPT)$_2$]** (FDPT = 5-fluoro-2,diphenylbenzene-1,4-dicarboxylate). Both **LMAs** undergo pressure induced switching transformations from non-porous to porous via adsorption of N_2, CO_2 and C_2H_2. **LMA-1** exhibited multi-step adsorption while **LMA-2** showed a single-step adsorption isotherm. The light responsive nature of the BTPC ligand in both frameworks was exploited with irradiation of **LMA-1** resulting in a 55 % maximum reduction of CO_2 uptake at 298 K. This study reports the first example of a switching sorbent (closed to open) that can be further modulated by light.

Introduction

State-of-the-art gas storage and delivery technologies are energy intensive, creating a need for alternative approaches which offer lower energy footprints.[1,2] Physisorption by stimuli-responsive porous coordination networks (PCNs) that switch between closed (non-porous) and open (porous) phases represents an emerging field of study that offers promise in this context.[3,4] Unlike most rigid PCNs with Type I gas sorption isotherm profiles (Figure 1a, top), such PCNs can exhibit[5] what we have termed Type F-IV isotherms,[6–8] which can offer working capacities equal to total uptake if the step occurs between the desired loading and delivery pressures (Figure 1a, bottom). Such sorbents also offer promise for utility in other technologies including as controlled release agents, responsive coatings or adaptive shape memory materials.[9,10] To the best of our knowledge, of the approximately 100 switching FMOMs reported to date,[11] only a handful have been subjected to systematic crystal engineering studies and none of these contain photo-responsive components.[12–14]

Photo-responsive molecules are classified in two ways: light-induced excitation with retention of structure or structural transformation induced by photon absorption (i.e. a molecular switch).[9,15–17] The well-studied latter category

[*] D. C. Castell,[+] V. I. Nikolayenko,[+] D. Sensharma, K. Koupepidou, M. J. Zaworotko
Department of Chemical Sciences, Bernal Institute, University of Limerick
Limerick V94T9PX (Republic of Ireland)
E-mail: xtal@ul.ie
K. A. Forrest, B. Space
Department of Chemistry, University of South Florida
Tampa, FL 33620-5250 (USA)
C. J. Solanilla-Salinas, B. Space
Department of Chemistry, North Carolina State University
Raleigh, NC 27607 (USA)
L. J. Barbour
Department of Chemistry and Polymer Science, University of Stellenbosch
Matieland 7600 (South Africa)
[+] These authors contributed equally to this work

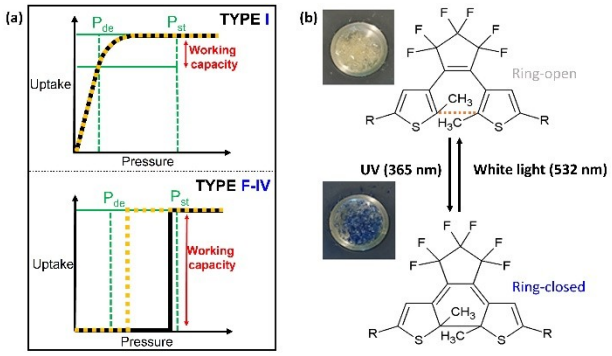

Figure 1. a) Comparison of Type I (top) and Type F-IV (bottom) physisorbent isotherm types. Desorption profiles are shown as dashed yellow lines. Type F-IV isotherms exhibit higher working capacities when compared to Type I sorbents. b) Reversible photocyclization of bis-3-thienylcyclopentenes using ultraviolet and white light. The structural transformation is concomitant with a color change from colorless to blue.

offers potential utility in light modulated adsorbents (LMAs), but the tendency of excited states to spontaneously undergo thermal isomerization back to their ground states means that a limited number of examples, azobenzenes (ABs),[18–21] spirobenzopyrans,[22,23] fulgides[23,25] and the [2+2] cycloaddition reactions in alkenes[26–29] have been studied in the solid-state. Furthermore, extracting structural information on materials exhibiting such dynamic behaviour can be hindered by crystal fracturing after phase transformations. Irie's work on bis-3-thienylcyclopentenes (BTCPs, Figure 1b) revealed that such molecules, when irradiated by ultraviolet (UV) light, can undergo photocyclization (concomitant with a colour change from colourless to blue) in the solid-state to yield thermally stable ring-closed isomers.[30] Cycloreversion (to the ring open form) may be induced by exposure to light of a higher wavelength with previous studies showing relatively high thermal stability and solid-state fatigue resistance of both isomers.[31]

For ring-closure to occur, the non-bonded distance between reactive carbon atoms (Figure 1, orange dashed line) should be less than 4 Å, while the presence of the fluorinated cyclopentene ring is believed to enhance reversibility and inhibit degradation.[32]

A primary goal of incorporating light-responsive components into PCNs is to translate the isomerization of photoactive molecules into changes in the macroscopic properties of the bulk molecular solid. In particular, the remote control and photo-switching of gas adsorption in solid sorbents could enhance kinetics, while decreasing the energy needed for cycling. This has previously been attempted through photochromic guests in framework cavities,[25] linker ligands with pendant AB or BTCP sidearms[19,20] or grafting of such moieties into either cages or framework backbones.[33–40] Although the latter category has the potential to produce the most pronounced structural changes, tethering reduces conformational freedom and mobility, requiring judicious linker selection (BTCP ligands are thus more optimal than AB ligands). Nevertheless, of the 58 ring-closed BTCP structures reported in the Cambridge Structural Database (CSD),[41] only two entries are porous sorbents wherein BTCP was used to modulate gas sorption.[34,35] Neither example exhibited a Type F-IV switching (closed-open) isotherm.

Herein, we expand on the previous pioneering studies performed on such porous solids and employ a strategic crystal engineering design approach to control the switching behavior of two light modulated adsorbents (LMA) and elucidate a mechanistic understanding of this behavior through structural and computational studies.

Results and Discussion

Large colorless hexagonal crystals of [Cd(BTCP)-(DPT)$_2$·3DMF], **LMA-1-α**, and [Cd(BTCP)(FDPT)$_2$·3DMF], **LMA-2-α**, (H_2DPT = 2,5-diphenylbenzene-1,4-dicarboxylic acid, H_2FDPT = 5-fluoro-diphenylbenzene-1,4-dicarboxylic acid, BTCP = 1,2 bis[2-methyl-5-(4-pyridyl)-3-thienyl]perfluorocyclopentene) were obtained through solvothermal reaction of $Cd(NO_3)_2$·$4H_2O$ with BTCP and either H_2DPT or H_2FDPT in a solution of ethanol and *N,N*-dimethylformamide (DMF).

To aid with visualization, these ligands have been simplified into node and linker representations (Figure S1) and used as such in all subsequent packing diagrams (Figure 2). Single crystal X-ray diffraction (SCXRD) analysis revealed that **LMA-1-α** and **LMA-2-α** are isostructural, both having crystallized in the space group $P2_1/c$ (Table S1) with one cadmium cation, two half DPT (or two half FDPT) ligands, one BTCP ligand and three DMF guest molecules per asymmetric unit (ASU).[42] Each cadmium molecular building block (MBB, Figure S2–S3) extends to form a 3D non-interpenetrated network with 8-c **hex** topology (Figure S4).

In **LMA-1-α**, DMF occupied channels account for 27 % of unit cell volume (determined using a Connolly map[43,44] with a 1.5 Å probe radius, Figure 2 top) and are separated by the presence of DPT ligands rotated into the *a*-axis while DPT ligands located at the apex of each channel are oriented along the *c*-axis (Figures 2, S4). The channels in **LMA-2-α** account for 32 % of unit cell volume and, unlike in **LMA-1-α**, the FDPT ligands orient diagonally to the *a*-axis connecting two channels into one at regular intervals (Figure 2, S4). The FDPT ligands at the apex of each channel remain oriented along the *c*-axis. The distances between the two photoactive carbon atoms in **LMA-1-α** and **LMA-2-α** are 3.708(9) and 3.621(4) Å, respectively.

When crystals of **LMA-1-α** were soaked in dichloromethane (DCM), they underwent rapid striation and SCXRD analysis revealed the formation of a new phase (**LMA-1-β**, Figure 2) with the space group unchanged but with the *b*-axis reduced by 1.2 Å and the unit cell volume by 11 % (Table S1). This transformation can be ascribed to rotation of the DPT ligand, which was previously oriented into the *a*-axis and now points diagonally along the *c*-axis, dividing the corrugated channels into isolated cavities that account for 21 % of unit cell volume (Figure 2). Although the DCM guest molecules could not be modelled crystallographically, the residual electron density analysis, as implemented by the SQUEEZE[45] routine of PLATON,[46] indicated the presence of two DCM molecules per ASU. The distance between the two photoactive carbon atoms in **LMA-1-β** remains almost unchanged (3.708(2) Å). Soaking **LMA-2-α** in DCM induced immediate powdering and thus **LMA-2-β** was not studied further.

When heat or vacuum was applied to **LMA-1-β or LMA-2-α** they underwent an additional structural transformation to the non-porous forms **LMA-1-γ1** and **LMA-2-γ1** (Figure 2). Both sorbents were found to be isostructural with further reductions in the *b*-axis length and unit cell volume. The beta angles increased by 10.2° and 15.42° respectively. This concertina-type contraction resulted from cleaving of one of the previously chelating DPT (or FDPT) ligands to mono-coordinate. In the presence of air, the coordinatively unsaturated metal was found to be occupied by an aqua ligand and, in the case of **LMA-1-γ1**, one guest water molecule was located. It should be noted that the transformations observed in **LMA-2** caused fragmentation of the

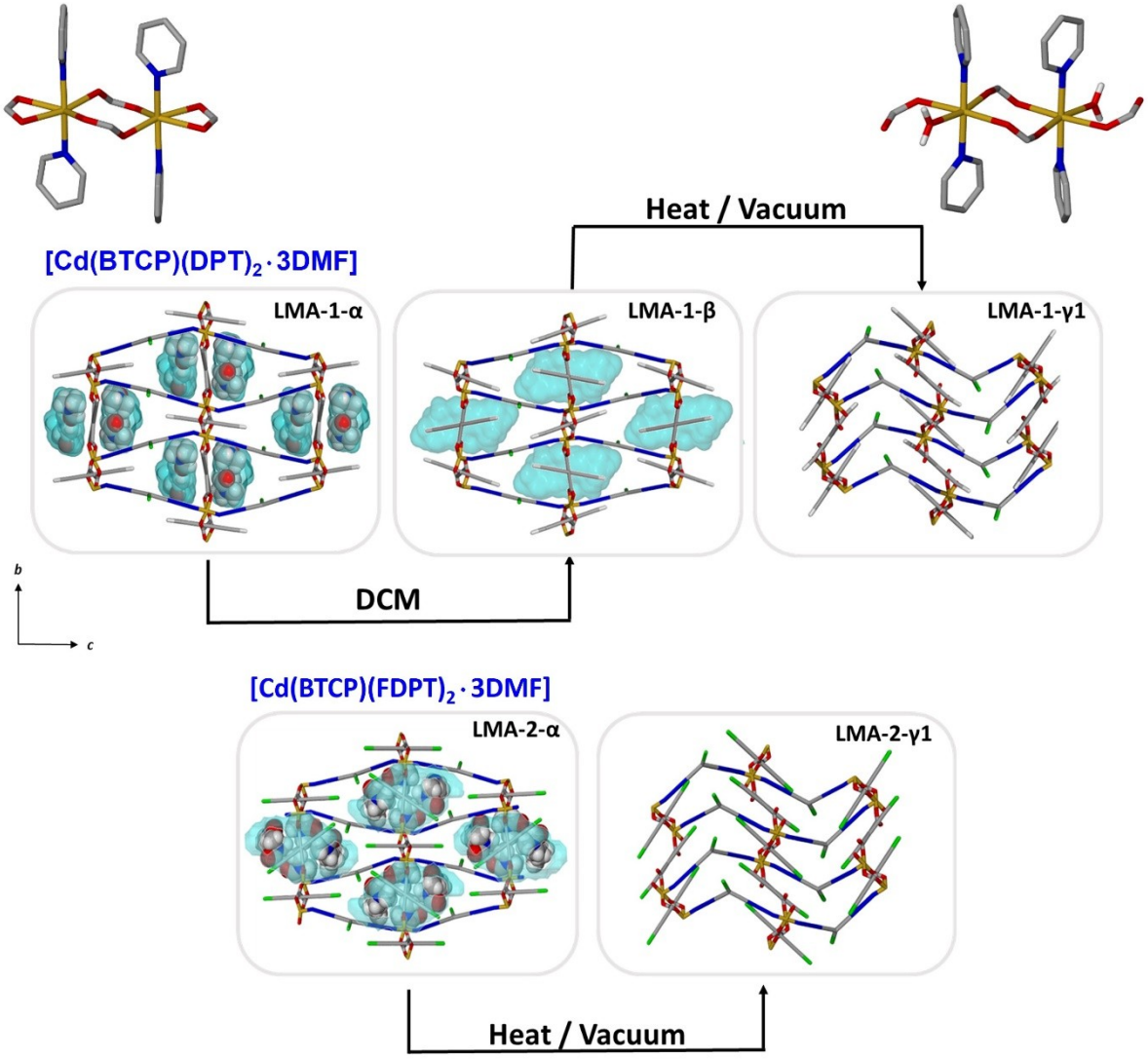

Figure 2. Node and linker depiction of structural transformations experienced by **LMA-1** (top) and **LMA-2** (bottom) upon guest exchange and activation in air. Inset (top left and top right) shows the effect activation imparts on the cadmium SBB (breaking of the chelating DPT bond and water insertion). Guest molecules are shown in space fill while guest accessible surfaces are shown in light blue and were mapped using a 1.5 Å probe radius.

single crystals. The resulting powder was shown to be microcrystalline by powder X-ray diffraction (PXRD). Another notable feature of these transformations is that the reactive C···C distance in **LMA-1-γ1** and **LMA-2-γ1** decreased to 3.486(2) and 3.564(4) Å, respectively. This reduction, coupled with the better crystal quality, prompted us to study the effect of ultra-violet (UV) light upon **LMA-1-γ1**. The photomicrographs in Figure 3a show that upon irradiation with UV light, an initially colorless single crystal of **LMA-1-γ1** changed color to dark blue within seconds (see animation S1 for real-time cycling). This color change can be attributed to the formation of a C–C bond between the two reactive carbon atoms in the BTCP linker. This transformation was found to be reversible with the application of light of a higher wavelength as evidenced by reversion of crystal color from dark blue to colorless (Figure 3a, animation S1). Inspection of the **LMA-1-γ1-UV** crystal structure revealed that the reactive C···C distance is now a C–C bond of 1.701(6) Å. Furthermore, the *a*- and *b*-axes exhibited an increase, while the *c*-axis and beta angle decreased. The structure is non-porous and to the best of our knowledge is only the third ring-closed BTCP SCXRD structure incorporated into a PCN reported to date.[34,35]

PXRD (Figures S8–S12), thermogravimetric analysis (TGA, Figures S13–S14) and Fourier transform Infrared spectroscopy (FTIR, Figure S15–S16) experiments are consistent with SCXRD data. Variable temperature PXRD experiments under nitrogen flow (Figures S17–S18) on both **LMA-α** forms confirmed that these as-synthesized phases can directly transform to guest-free **LMA-γ2** (no coordinated aqua ligands). In both cases, with increased heating (in the temperature range of guest-loss observed in TGA

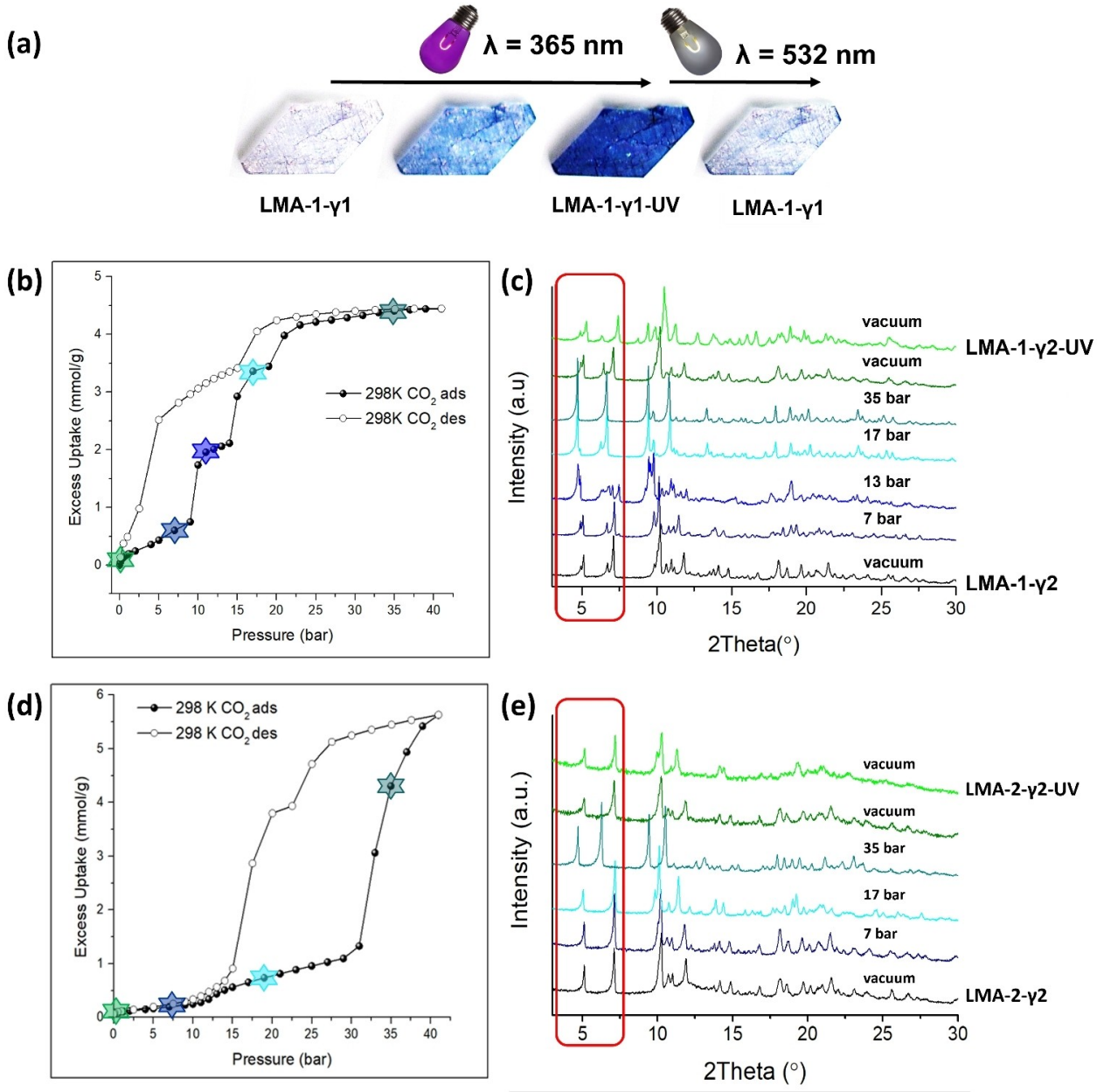

Figure 3. (a). Photomicrographs of a crystal of **LMA-1-γ1** irradiated with UV light (365 nm) and then with white light (532 nm). High pressure CO_2 sorption isotherms for (b) **LMA-1-γ2** and (d) **LMA-2-γ2** collected at 298 K with pressures of interest shown as coloured stars on the isotherms. Selected pressures corresponding to in situ CO_2-loaded PXRD patterns for (c) **LMA-1-γ2** and (e) **LMA-2-γ2**. Light green PXRDs are for both materials irradiated with UV light.

experiments) PXRD peaks were observed to shift to higher 2θ values, which is consistent with contraction of the unit cell. The PXRD diffractograms of both sorbents measured at 200 °C show some peak splitting. Without the SCXRD of **LMA-γ2** to provide a reference PXRD, the origin of the observed peak splitting and variances between **LMA-γ1** and **LMA-γ2** cannot be verified. Overall, the PXRDs at 25 °C match well with those obtained for each phase under vacuum (see Supporting Information section 9 for details). To further investigate the phase behavior of both **LMA-γ2** sorbents over a broad P/P_0 range, low temperature 77 K N_2, 195 K CO_2, and 195 K C_2H_2 gas sorption experiments were performed. **LMA-1-γ2** underwent a switching (closed to open) phase transition with a threshold pressure of 0.16 bar while no appreciable N_2 uptake was observed for **LMA-2-γ2** (Figure S19–S20). In the case of CO_2, **LMA-1-γ2** underwent a 2-step transformation with a threshold pressure of 0.02 bar (Figure S21a) while **LMA-2-γ2** underwent single-step conversion with an inflection at higher partial pressure (0.07 bar, Figure S22a). The recyclability of both materials was investigated using CO_2 at 195 K. After four cycles of adsorption-desorption, no reduced performance was ob-

served (Figure S21b and S22b). The total uptake and effective working capacity (0.1–1 bar) for **LMA-1-γ2** is about 114 cc g^{-1} (STP) and 67 cc g^{-1} (STP) respectively, while for **LMA-2-γ2** it is 128 cc g^{-1} and 121 cc g^{-1}. Upon exposure to C_2H_2, **LMA-1-γ2** underwent a 3-step transformation with a threshold pressure of 0.01 bar while **LMA-2-γ2** exhibited initial loading of 0.5 mmol at 0.02 bar, followed by a second step at 0.03 bar (Figures S23–S24). A comparison of all six isotherms shows that **LMA-1-γ2** underwent switching at lower partial pressures than **LMA-2-γ2**. Furthermore, **LMA-1-γ2** exhibited two intermediate phases between closed and open while **LMA-2-γ2** did not. Although the **LMA-γ2** forms are isostructural, the substitution of fluorine for the hydrogen atom in DPT clearly influenced the sorption properties of the material. The single point pore volumes obtained from these cryogenic sorption experiments (Table S2) correlate well with pore volumes from SCXRD (Table S3).

High-pressure CO_2 gas sorption experiments were collected at 273 K and 298 K (Figure 3b and 3d) and showed good agreement with the cryogenic data (Figures S25–S26), in particular the high-pressure CO_2 isotherm profiles collected at 298 K vs. the C_2H_2 195 K data. To gain further insight into the nature of the transformations of the **LMA-γ2** forms, in situ PXRD experiments at selected pressures were performed (see Supporting Information for details). At 7 bar CO_2, the PXRD patterns of both **LMA-γ2** forms (Figure 3c and 3e) revealed peak shifting to lower 2θ values consistent with expansion of the unit cell volume with a phase change occurring at 13 bar for **LMA-1**. At this pressure, the first PXRD peak had shifted to $2\theta = 4.75°$ with additional new peaks occurring at $2\theta = 6.35°$, 7.31°, 9.46°, 10.40° and 19.01°.

The good pore volume agreement (Table S2–S3) of **LMA-1-γ2** suggests that this CO_2-loaded phase may be equivalent to **LMA-1-β**. At 17 bar, a second transformation was observed in **LMA-1** with peaks shifting to even lower 2θ values. Four prominent peaks were observed at $2\theta = 4.75°$, 6.75°, 9.44° and 10.91°. Unlike **LMA-1**, **LMA-2** did not transform at this pressure. Further loading (35 bar) for **LMA-1** showed only minor peak shifting, this phase being similar to **LMA-1-α** but with CO_2 as the guest. In the case of **LMA-2**, the PXRD pattern at 35 bar was markedly different to that at 17 bar but matched that of **LMA-1**. Upon exposure to vacuum, both sorbents reverted to the respective **LMA-x-γ2** phases.

Having observed ring-closure in a single crystal of **LMA-1**, the effect of ring-closure upon the sorption properties of **LMA-1-γ2** was investigated by continuously irradiating a bulk powder sample for six hours. The nature of the sorption and XRD photoirradiation experiments required that the data were collected on **LMA-1-γ2** and **LMA-1-γ1**, respectively. An overlay of the PXRD pattern generated from the SCXRD of **LMA-1-γ1-UV** with the experimentally obtained PXRD pattern of **LMA-1-γ2-UV** obtained using an environment cell (Figure S31) is consistent with isostructural but different crystal structures. The previously colorless sample turned dark blue and the PXRD diffractogram showed peak shifting to higher 2θ values consistent with contraction of the unit cell volume. New peaks were observed at $2\theta = 8.79°$, 12.60° and 13.81° (Figure 3c, light green). Progressive loading of this phase with 7, 14 and 21 bar of CO_2 showed no changes in the PXRD pattern (Figure S29). This implies that the ring-closed **LMA-1-γ2-UV** form is stable and not subject to structural reopening under the pressure range studied.

This assumption was further investigated by reversibly irradiating a bulk sample of **LMA-1-γ2** (see Supporting Information for details) and collecting cryogenic and high-pressure CO_2 experiments at 195 K and at 298 K. Owing to experimental design limitations (relating to sample type, size and irradiation source availability), the powdered sample had to be continuously irradiated for several days (see Supporting Information for details). Figure S30 reveals that depending on the extent of irradiation **LMA-1-γ2-UV** can reversibly reduce its loading capacity by 30–55 %.

With the focus of gaining further insight into why a single atom substitution (from hydrogen to fluorine) creates such a marked difference in sorption properties, a computational study was performed. Periodic density functional theory (DFT) electronic structure minimizations were performed on the experimental crystal structures of **LMA-1-α**, **LMA-1-β**, and **LMA-2-α** desolvated in silico to assess their structural relaxation and intermediates. **LMA-1-α** was found to smoothly relax to a γ-like structure, while **LMA-1-β** relaxed to a metastable open state, with notable changes to its crystal structure but no collapse. Interestingly **LMA-2-α**, while crystallographically similar in volume and lattice parameters to **LMA-1-α**, shares more structural similarities with **LMA-1-β** and as such, is also stabilized from collapse (Animations S2–4, Figures S33–S34).

These relaxations illustrate several key points. **LMA-1-α**'s crystal structure has a central DPT linker positioned along the *a*-axis surrounded by 4 BTCP linkers. Its optimization into a γ-like structure results from three cooperative movements: rotation of the DPT linker; extension of two N–Cd bonds and displacement of the fluorinated backbone rings of the BTCP linkers. The empty space on either side of the DPT linker permits facile rotation around its central axis, defined by the Cd-carboxylate bonds on either end. At the onset of rotation, two N–Cd bonds from the terminal ends of BTCP linkers and cadmium nodes extend and shift from their original position, moving closer to the center of the pore. As the pore volume decreases, the terminal phenyl rings rotate towards the perfluorinated backbone on the BTCP linkers. The perfluorinated backbones shift away from the incoming DPT linker, triggering the collapse into a γ-like structure (Animation S2).

Furthermore, both **LMA-1-β** and **LMA-2-α** have a central DPT/FDPT linker positioned diagonally across their respective pores along the *b*-axis. If the 4 BTCP linkers are taken to be the walls of a pore, the central DPT linker in **LMA-1-β** has its *para*-hydrogen positioned outside of the pore walls at a distance of 3.91 Å away from the nearest BTCP fluorine (Figure S35). The resulting forces cause the rotation of the DPT linker to turn away from the fluorinated rings until it plateaus at an energy minimum with a position 7.53 Å away from the nearest BTCP fluorine. This motion, along with the lack of empty space, allows a rotation

analogous to that present in **LMA-1-α**. This leads to no extension of the N–Cd bonds and no displacement of the fluorinated rings on the BTCP linkers, resulting in a metastable open state (Animation S3).

LMA-2-α has its central FDPT linker also positioned diagonally but protruding into the pore walls, at a distance of 2.86 Å away from the nearest BTCP fluorine (Figure S36). This restricted pore space prevented large cooperative movements to take place, leaving the structure in an open state with small changes to atom positions after optimization (Animation S4). Although **LMA-2-α** has been shown to collapse into its γ-structure experimentally, it is postulated that this is only possible with external perturbations sufficient to overcome the energetic barrier presented by inherent steric hindrance, such as the movement of guest molecules during desorption.

These results demonstrate a readily accessible energy landscape for different phases of **LMA-1** and support the experimentally observed behavior of **LMA-1's** sorption isotherm being multi-step in contrast to **LMA-2**. The DPT moiety in **LMA-1** allows access to a variety of states from the open to closed phase as shown by the relaxation of **LMA-1-α**. Relaxation of **LMA-1-β** also showed the presence of metastable states that could correspond to distinct steps on the sorption isotherm. (Figure S33, S34). The physically relevant nature of the conformational states were assessed by the simulated excess adsorption isotherms of **LMA-1-α** and **LMA-2-α** (Table S4) confirming similar uptake at saturation, and for **LMA-1-β**, uptake characteristic of a state corresponding to a step in the isotherm.

From this data, it is inferred that fluorination of the DPT linker leads to a more sterically frustrated open phase in **LMA-2**, with an energy barrier associated with collapse that was not observed from the relaxation calculations of **LMA-1**. This behavior mirrors the sharp transition from the closed to the open phase shown in **LMA-2's** single-step sorption isotherm.

Conclusion

In summary, we present the first example of a family of light modulated adsorbents (LMAs) which reversibly switch (closed to open phase transformation) in response to multiple stimuli (i.e. gas/vapor and heat/vacuum) and which have light-responsive components incorporated into the backbone of the PCN, enabling a further ring-open to ring-closed transformation. In addition to bulk conversion in the form of powdered sorbent, we include a mechanistic understanding of the bulk conversion in large particles (i.e. single crystals). This insight, coupled with the effect single-atom substitution imparts on the host–guest interactions of these sorbents, enabled us to characterize a sorbent with improved performance (single-step switching with increased loading). Furthermore, the incorporated UV modulated molecular switch suggests an energy efficient method of desorption under ambient conditions. The study serves as a proof of concept for the development of light-responsive PCNs in gas storage.

Acknowledgements

The authors gratefully acknowledge support from *Molecule RnD Ltd.* (Nexus Innovation Centre), the Irish Research Council (IRCLA/2019/167), the European Research Council (ADG 885695), Science Foundation Ireland (16/IA/4624 and 12/RC/2278 P2). The authors also appreciate the financial support of the National Research Foundation of South Africa. K. A. F., C. J. S. S., and B. S. also acknowledge support from the Hydrogen and Fuel Cell Technologies and Vehicle Technologies Office within the U.S. Department of Energy's Office of Energy Efficiency and Renewable Energy (Award No. DE-EE0008812). Computational resources were made available by a XSEDE grant (No. TG-DMR090028) as well as High-Performance Computing at NC State. Open Access funding provided by IReL.

Conflict of Interest

The authors declare no conflict of interest.

Data Availability Statement

The data that support the findings of this study are available in the Supporting Information of this article.

Keywords: Gas-Sorption · Photochromism · SCXRD · Stimuli-Responsive Compounds · Switching

[1] S. Yeh, *Energy Policy* **2007**, *35*, 5865–5875.
[2] S. Chu, A. Majumdar, *Nature* **2012**, *488*, 294–304.
[3] S. Horike, S. Shimomura, S. Kitagawa, *Nat. Chem.* **2009**, *1*, 695–704.
[4] J. A. Mason, J. Oktawiec, M. K. Taylor, M. R. Hudson, J. Rodriguez, J. E. Bachman, M. I. Gonzalez, A. Cervellino, A. Guagliardi, C. M. Brown, P. L. Llewellyn, N. Masciocchi, J. R. Long, *Nature* **2015**, *527*, 357–361.
[5] F. X. Coudert, *Chem. Mater.* **2015**, *27*, 1905–1916.
[6] H. Kanoh, A. Kondo, H. Noguchi, H. Kajiro, A. Tohdoh, Y. Hattori, W.-C. Xu, M. Inoue, T. Sugiura, K. Morita, H. Tanaka, T. Ohba, K. Kaneko, *J. Colloid Interface Sci.* **2009**, *334*, 1–7.
[7] Q.-Y. Yang, P. Lama, S. Sen, M. Lusi, K.-J. Chen, W.-Y. Gao, M. Shivanna, T. Pham, N. Hosono, S. Kusaka, J. J. Perry IV, S. Ma, B. Space, L. J. Barbour, S. Kitagawa, M. J. Zaworotko, *Angew. Chem. Int. Ed.* **2018**, *57*, 5684–5689; *Angew. Chem.* **2018**, *130*, 5786–5791.
[8] C. M. Simon, J. Kim, D. A. Gomez-Gualdron, J. S. Camp, Y. G. Chung, R. L. Martin, R. Mercado, M. W. Deem, D. Gunter, M. Haranczyk, D. S. Sholl, R. Q. Snurr, B. Smit, *Energy Environ. Sci.* **2015**, *8*, 1190–1199.
[9] R. Haldar, L. Heinke, C. Wöll, *Adv. Mater.* **2020**, *32*, 1905227.
[10] Y. Ru, Z. Shi, J. Zhang, J. Wang, B. Chen, R. Huang, G. Liu, T. Yu, *Mater. Chem. Front.* **2021**, *5*, 7737–7758.
[11] S. Q. Wang, S. Mukherjee, M. J. Zaworotko, *Faraday Discuss.* **2021**, *231*, 9–50.
[12] N. Nijem, H. Wu, P. Canepa, A. Marti, K. J. Balkus, T. Thonhauser, J. Li, Y. J. Chabal, *J. Am. Chem. Soc.* **2012**, *134*, 15201–15204.

[13] S. Q. Wang, S. Darwish, D. Sensharma, M. J. Zaworotko, *Mater. Adv.* **2022**, *3*, 1240–1247.
[14] A. X. Zhu, Q. Y. Yang, S. Mukherjee, A. Kumar, C. H. Deng, A. A. Bezrukov, M. Shivanna, M. J. Zaworotko, *Angew. Chem. Int. Ed.* **2019**, *58*, 18212–18217; *Angew. Chem.* **2019**, *131*, 18380–18385.
[15] W. Danowski, T. van Leeuwen, W. R. Browne, B. L. Feringa, *Nanoscale Adv.* **2021**, *3*, 24–40.
[16] N. D. Shepherd, D. M. D'Alessandro, *Chem. Phys. Rev.* **2021**, *2*, 011301–011315.
[17] F. Xu, B. L. Feringa, *Adv. Mater.* **2023**, *35*, 202204413.
[18] R. Lyndon, K. Konstas, B. P. Ladewig, P. D. Southon, C. J. Kepert, M. R. Hill, *Angew. Chem. Int. Ed.* **2013**, *52*, 3695–3698; *Angew. Chem.* **2013**, *125*, 3783–3786.
[19] Z. Wang, K. Müller, M. Valášek, S. Grosjean, S. Bräse, C. Wöll, M. Mayor, L. Heinke, *J. Phys. Chem. C* **2018**, *122*, 19044–19050.
[20] J. Park, D. Yuan, K. T. Pham, J. R. Li, A. Yakovenko, H. C. Zhou, *J. Am. Chem. Soc.* **2012**, *134*, 99–102.
[21] S. Krause, J. D. Evans, V. Bon, S. Crespi, W. Danowski, W. R. Browne, S. Ehrling, F. Walenszus, D. Wallacher, N. Grimm, D. M. Többens, M. S. Weiss, S. Kaskel, B. L. Feringa, *Nat. Commun.* **2022**, *13*, 1951.
[22] M. Kamenjicki Maurer, I. K. Lednev, S. A. Asher, *Adv. Funct. Mater.* **2005**, *15*, 1401–1406.
[23] S. Kremer, I. Ober, V. Greussing, H. Kopacka, H. G. Gallmetzer, B. Trübenbacher, D. Demmel, S. Olthof, H. Huppertz, H. A. Schwartz, *Langmuir* **2022**, *38*, 4295–4309.
[24] V. Greussing, J. M. Gallmetzer, H. Huppertz, T. S. Hofer, H. A. Schwartz, *J. Phys. Chem. C* **2022**, *126*, 10923–10931.
[25] C. Eichler, A. Rázková, F. Müller, H. Kopacka, H. Huppertz, T. S. Hofer, H. A. Schwartz, *Chem. Mater.* **2021**, *33*, 3757–3766.
[26] G. M. J. Schmidt, *Pure Appl. Chem.* **1971**, *27*, 647–678.
[27] S. P. Yelgaonkar, G. Campillo-Alvarado, L. R. MacGillivray, *J. Am. Chem. Soc.* **2020**, *142*, 20772–20777.
[28] B. Bhusan Rath, J. J. Vittal, *J. Am. Chem. Soc.* **2020**, *142*, 20117–20123.
[29] D. A. Sherman, R. Murase, S. G. Duyker, Q. Gu, W. Lewis, T. Lu, Y. Liu, D. M. D'Alessandro, *Nat. Commun.* **2020**, *11*, 2808.
[30] S. Kobatake, S. Takami, H. Muto, T. Ishikawa, M. Irie, *Nature* **2007**, *446*, 778–781.
[31] M. Irie, T. Fukaminato, K. Matsuda, S. Kobatake, *Chem. Rev.* **2014**, *114*, 12174–12277.
[32] J. Zhang, H. Tian, *Adv. Opt. Mater.* **2018**, *6*, 1701278.
[33] J. Dong, V. Wee, D. Zhao, *Nat. Mater.* **2022**, *21*, 1334–1340.
[34] V. I. Nikolayenko, S. A. Herbert, L. J. Barbour, *Chem. Commun.* **2017**, *53*, 11142–11145.
[35] Y. Zheng, H. Sato, P. Wu, H. J. Jeon, R. Matsuda, S. Kitagawa, *Nat. Commun.* **2017**, *8*, 100.
[36] M. Han, R. Michel, B. He, Y.-S. Chen, D. Stalke, M. John, G. H. Clever, *Angew. Chem. Int. Ed.* **2013**, *52*, 1319–1323; *Angew. Chem.* **2013**, *125*, 1358–1362.
[37] R.-J. Li, J. Tessarolo, H. Lee, G. H. Clever, *J. Am. Chem. Soc.* **2021**, *143*, 3865–3873.
[38] K. Artmann, R.-J. Li, S. Juber, E. Benchimol, L. V. Schäfer, G. H. Clever, P. Nuernberger, *Angew. Chem. Int. Ed.* **2022**, *61*, e202212112; *Angew. Chem.* **2022**, *134*, e202212112.
[39] M. Ovalle, M. Kathan, R. Toyoda, C. N. Stindt, S. Crespi, B. L. Feringa, *Angew. Chem. Int. Ed.* **2022**, *61*, e202214495; *Angew. Chem.* **2022**, *134*, e202214495.
[40] I. E. Claassens, V. I. Nikolayenko, D. A. Haynes, L. J. Barbour, *Angew. Chem. Int. Ed.* **2018**, *57*, 15563–15566; *Angew. Chem.* **2018**, *130*, 15789–15792.
[41] C. R. Groom, I. J. Bruno, M. P. Lightfoot, S. C. Ward, *Acta Crystallogr. Sect. B* **2016**, *72*, 171–179.
[42] Deposition numbers 2220878, 2220879, 2220880, 2220881, 2220882 and 2220883 contain the supplementary crystallographic data for this paper. These data are provided free of charge by the joint Cambridge Crystallographic Data Centre and Fachinformationszentrum Karlsruhe Access Structures service.
[43] M. L. Connolly, *J. Mol. Graphics* **1993**, *11*, 139–141.
[44] M. L. Connolly, *Science* **1983**, *221*, 709–713.
[45] A. L. Spek, *Acta Crystallogr. Sect. D* **2009**, *65*, 148–155.
[46] A. L. Spek, *Acta Crystallogr. Sect. C* **2015**, *71*, 9–18.

Manuscript received: December 26, 2022
Accepted manuscript online: March 6, 2023
Version of record online: ■■, ■■

Research Articles

Porous Materials

D. C. Castell, V. I. Nikolayenko, D. Sensharma, K. Koupepidou, K. A. Forrest, C. J. Solanilla-Salinas, B. Space, L. J. Barbour, M. J. Zaworotko* _____ **e202219039**

Crystal Engineering of Two Light and Pressure Responsive Physisorbents

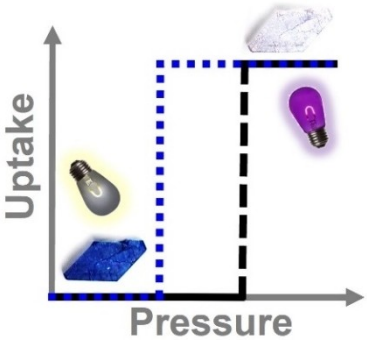

An emerging strategy to enable energy efficient gas storage and separation technologies is the development of stimuli-responsive physisorbents. Herein, we report two isostructural light-modulated adsorbents (LMAs) which undergo pressure-induced transformations from closed (non-porous) to open (porous) phases via adsorption of N_2, CO_2 and C_2H_2.